The Astronomical Journal, 159:184 (8pp), 2020 April https://doi.org/10.3847/1538-3881/ab7cd5

The Origin of Neptune's Unusual Satellites from a Planetary Encounter

Daohai Li[1] and Apostolos A. Christou[2]
[1] Lund Observatory, Department of Astronomy and Theoretical Physics, Lund University, Box 43, SE-221 00 Lund, Sweden; lidaohai@gmail.com, li.daohai@astro.lu.se
[2] Armagh Observatory and Planetarium, College Hill, Armagh, BT61 9DG, Northern Ireland, UK
Received 2019 December 7; revised 2020 February 27; accepted 2020 March 3; published 2020 April 1

Abstract

The Neptunian satellite system is unusual, comprising Triton, a large (∼2700 km) moon on a close-in, circular, yet retrograde orbit, flanked by Nereid, the largest irregular satellite (∼300 km) on a highly eccentric orbit. Capture origins have been previously suggested for both moons. Here we explore an alternative in situ formation model where the two satellites accreted in the circum-Neptunian disk and are imparted irregular and eccentric orbits by a deep planetary encounter with an ice giant (IG), like that predicted in the Nice scenario of early solar system development. We use *N*-body simulations of an IG approaching Neptune to 20 Neptunian radii ($R_{\rm Nep}$), through a belt of circular prograde regular satellites at 10–30 $R_{\rm Nep}$. We find that half of these primordial satellites remain bound to Neptune and that 0.4%–3% are scattered directly onto wide and eccentric orbits resembling that of Nereid. With better matches to the observed orbit, our model has a success rate comparable to or higher than capture of large Nereid-sized irregular satellites from heliocentric orbit. At the same time, the IG encounter injects a large primordial moon onto a retrograde orbit with specific angular momentum similar to Triton's in 0.3%–3% of our runs. While less efficient than capture scenarios, our model does indicate that an in situ origin for Triton is dynamically possible. We also simulate the post-encounter collisional and tidal orbital evolution of Triton analog satellites and find they are decoupled from Nereid on timescales of $\sim 10^4$ yr, in agreement with Cuk & Gladman.

Unified Astronomy Thesaurus concepts: Satellite formation (1425); Neptunian satellites (1098); Irregular satellites (2027); Close encounters (255); Celestial mechanics (211)

1. Introduction

Observational biases notwithstanding, Neptune has the smallest number of satellites among the four giant planets but perhaps with the most intriguing orbits. The largest moon, Triton, is orbiting its host planet at 14 Neptunian radii ($R_{\rm Nep}$) on a circular path but, oddly, in a retrograde direction. Nereid, >200 $R_{\rm Nep}$ further out and the third largest moon in the system, has the highest orbital eccentricity among solar system moons (Figure 1).

Mechanisms favoring capture of Triton from heliocentric orbit include gas drag (McKinnon 1984; McKinnon & Leith 1995), collisions (Goldreich et al. 1989), and three-body gravitational interaction (Agnor & Hamilton 2006; Vokrouhlický et al. 2008; Nogueira et al. 2011). See Colombo & Franklin (1971), Heppenheimer & Porco (1977), Pollack et al. (1979), Ćuk & Burns (2004), Nicholson et al. (2008), and Nesvorný et al. (2007, 2014a) for discussions on satellite capture.

In an alternative in situ formation scenario, the two moons have accreted in the circum-Neptunian disk (e.g., Szulágyi et al. 2018) with initially circular, prograde orbits on the equatorial plane of Neptune. This raises the question of how they arrive at their current orbits.

Harrington & Van Flandern (1979) originally postulated an encounter between an ad hoc planetary body of several Earth masses and Neptune, flipping Triton's orbit and scattering Nereid outward. This scenario has been criticized (Farinella et al. 1980; McKinnon et al. 1995) on the grounds that the encountering planet is not observed in the solar system and that the encounter may have over-excited Neptune's orbit. Also, computational resources available at that time allowed only one "successful" simulation run, making it difficult to estimate the success rate of this particular evolutionary path. In a subsequent model where Triton was assumed captured, Goldreich et al. (1989) suggested that Nereid could be scattered onto a wide orbit by Triton, an outcome not reproduced in numerical simulations (Nogueira et al. 2011).

It is believed the giant planets radially migrated in the early solar system (Fernández & Ip 1984; Malhotra 1993) in the now widely accepted framework of the Nice model. There, the planets formed at different heliocentric distances from those where they are presently observed and, due to interactions with a primordial planetesimal disk (PPD), they migrated to their current locations. Since its introduction (Tsiganis et al. 2005), the Nice model has evolved considerably to meet an enhanced set of constraints. Because of the difficulty to correctly excite the orbit of Jupiter (Morbidelli et al. 2009) and, at the same time, to avoid over-exciting the inner main asteroid belt (Morbidelli et al. 2010; Minton & Malhotra 2011) and the terrestrial planets (Brasser et al. 2009; Agnor & Lin 2012), Jupiter is thought to have impulsively "jumped" over the 2:1 mean motion resonance with Saturn, owing to close encounters with an ice giant. As such, a five-planet variant of the Nice model, where an additional ice giant planet (IG hereafter) was subsequently ejected from the solar system, was introduced (Batygin et al. 2012; Nesvorný & Morbidelli 2012). The IG, before its ejection, probably encountered other planets as well, leading to the capture of Trojans and irregular satellites (Nesvorný et al. 2013, 2014a) and the emplacement of the so-called "kernel" of the Kuiper Belt (Nesvorný 2015). These planet–planet encounters may have been as close as 0.003 au (Nesvorný et al. 2014b), penetrating to the satellite region.

The appearance of the Nice scenario mitigates the two major objections (Farinella et al. 1980; McKinnon et al. 1995) to the in situ formation of Triton (Harrington & Van Flandern 1979) since the encountering IG could have been ejected from the solar system and thus be rendered unobservable while Neptune's

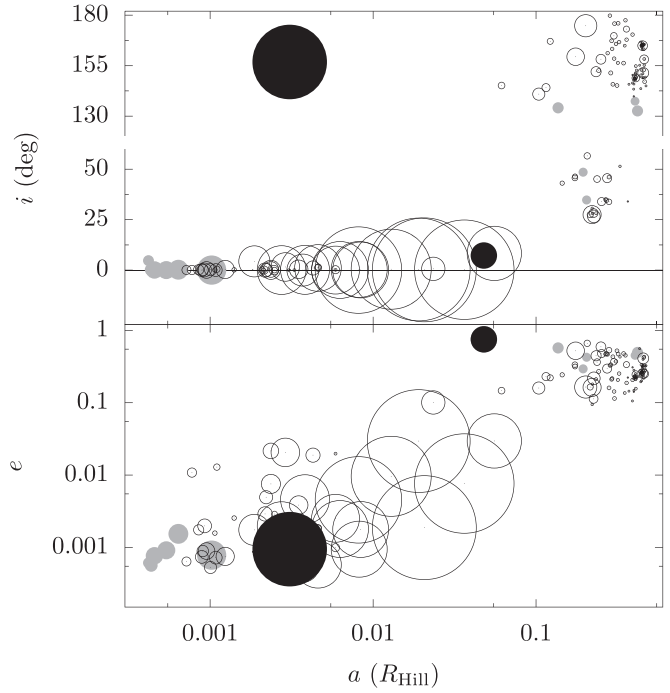

Figure 1. Distribution of giant planet moons in the (a, i) and (a, e) planes from Scott Sheppard's website: https://sites.google.com/carnegiescience.edu/sheppard/moons. Symbol size is proportional to the square root of that moon's actual size. Gray symbols represent moons around Neptune while Triton and Nereid are the large and small black filled circles respectively. Small (5–10×10^{-4}) vertical offsets have been added to allow moons with negligible orbital eccentricity to be displayed on a log-scale.

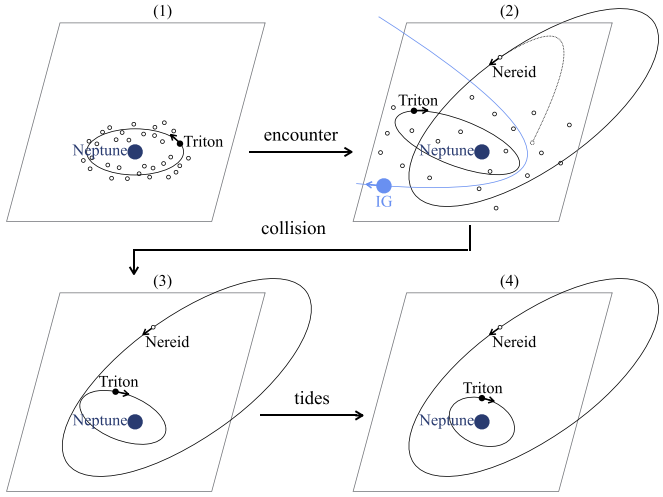

Figure 2. Illustration of our origin scenario for Triton and Nereid. Before the encounter, several tens of preexisting moons orbit Neptune (1), all small (open circles) except one that is Triton-sized (black filled circle). After the IG encounter (2), the orbit of the large moon is flipped and a small moon is emplaced onto a wide, eccentric orbit, turning into Nereid. Subsequently (3), collisions with Triton remove the other small moons and decouple the orbit of Triton from Nereid's. Finally (4), tides circularize Triton's orbit.

eccentricity, even if excited, may be damped owing to the interaction with the planetesimal disk (actually, the encounters considered here ensure that the orbit of Neptune is at most mildly excited). Hence it is worthwhile to reexamine the in situ formation model within the constraints of the Nice scenario, also providing statistics of successful versus unsuccessful simulation runs, to estimate model efficiency and explore the ensuing Neptunian system evolution post-encounter. We focus on studying how a close encounter between Neptune and the IG could bring about the unusual orbits of Triton and Nereid. Our model consists of three parts. First (Section 2), we check how the IG encounter scatters an initial population of Neptunian moons onto distant, eccentric orbits as well as onto retrograde orbits. In Section 3 we study the system's post-encounter evolution via collisions and tidal dissipation. The implications and conclusions are presented in Sections 4 and 5.

2. NEPTUNE-IG Encounter

Following Cloutier et al. (2015), and as detailed below, we first set up the ice giant (IG)-Neptune encounters; then the satellites' evolutions under these encounters are examined. See panels (1) and (2) of Figure 2 for an illustration of this phase.

2.1. Model

We consider a three-body system comprising the Sun, the IG, and Neptune. In order to fully control the minimum separation $d_{\rm enc}$ between the IG and Neptune, we start with the Sun-IG-Neptune system at the moment of the two planets' closest approach (Cloutier et al. 2015), i.e., when the relative position vector satisfies $|\boldsymbol{r}_{\rm IG-N}| = d_{\rm enc}$; we set $d_{\rm enc} = 0.003$ au (or 18 Neptunian radii Nesvorný et al. 2014b). At this moment, the relative velocity vector is perpendicular to the relative position vector: $\boldsymbol{v}_{\rm IG-N} \perp \boldsymbol{r}_{\rm IG-N}$. We further assume their relative kinetic energy $|\boldsymbol{v}_{\rm IG-N}|^2$ to be uniformly distributed within the range $(0, 3v_{\rm esc}^2)$, where $v_{\rm esc}$ is the two-body escape velocity between the IG and Neptune. The orientations of the two vectors are random in the solid angle. Then the IG-Neptune barycenter is assigned a heliocentric orbit parameterized by the set of orbital elements $(a_{\rm IG+N}, e_{\rm IG+N}, i_{\rm IG+N})$, with values within the ranges: $a_{\rm IG+N} \in (10, 40)$ au, $e_{\rm IG+N} \leqslant 0.7$, and $i_{\rm IG+N} \leqslant 10^\circ$; the angular elements are randomly drawn from a uniform distribution. We calculate the position and velocity vectors $\boldsymbol{r}_{\rm IG+N}$ and $\boldsymbol{v}_{\rm IG+N}$ and combine them with $\boldsymbol{r}_{\rm IG-N}$ and $\boldsymbol{v}_{\rm IG-N}$ to fully define the heliocentric state vectors of the IG and Neptune at the instant of closest approach. Next, we carry out a reference frame transformation such that the z-axis is parallel to the total angular momentum of the three-body system. We refer to this as the heliocentric frame. The IG mass is 18 Earth masses (Nesvorný et al. 2014b), similar to that of Neptune.

We integrate this system backwards and forwards for 10 yr apiece using the general Bulirsch–Stoer algorithm in MERCURY (Chambers 1999) with an error tolerance of 10^{-14}. At the end of these two integrations, we check the planets' mutual distance is larger than 0.8 au, Neptune's current Hill radius (see below). Then the heliocentric orbital elements of Neptune are used to determine whether an encounter is "realistic" in that its semimajor axis is in the range $25\,{\rm au} < a_{\rm N} < 30\,{\rm au}$ and eccentricity is $e_{\rm N} < 0.15$; For the inclination, we only require that the change in the direction of the heliocentric angular momentum vector before and after the encounter is $\Delta i_{\rm N} < 6^\circ$, for consistency with Nice scenario simulations (Nesvorný & Morbidelli 2012; Gomes et al. 2018) and with constraints derived from Neptune's perturbation on the Cold Kuiper Belt Objects (CKBOs; Dawson & Murray-Clay 2012; Wolff et al. 2012). We additionally require that the change in the Neptunian semimajor axis before and after the encounter is <1 au (Nesvorný 2015). While a more violent dynamical history of Neptune is not necessarily inconsistent with the CKBOs

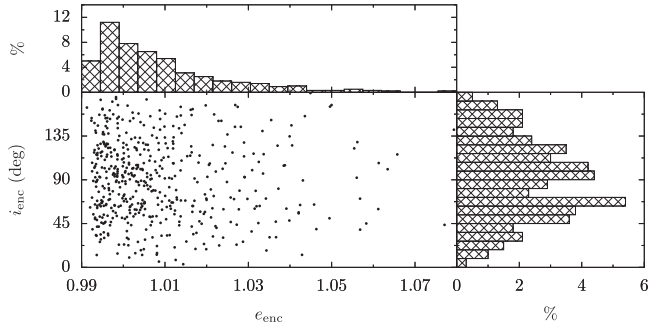

Figure 3. Distribution of eccentricity and inclination of the IG in the Neptune-centric frame, the latter measured wrt Neptune's equator. Histograms of the two quantities are shown in the top and right panels.

(Morbidelli et al. 2014; Gomes et al. 2018), the planets' exact heliocentric orbits are irrelevant for the satellites' evolution during the brief encounter. Furthermore, this encounter need not be the last one and subsequent encounters may additionally change the orbit of Neptune. Thus the Neptunian orbit in our simulations may not define the starting point of ensuing outward migration and damping in e and i, upon which the constraints from CKBOs were imposed (Dawson & Murray-Clay 2012).

A total of 500 encounters are generated in this way. In Figure 3, we show the distribution of the IG's orbit with respect to Neptune at closest approach. As expected (see Deienno et al. 2014), they are mostly near-parabolic due to strong gravitational focusing. The resemblance of the distribution of $i_{\rm enc}$ (measured in the Neptunian-centric frame, see below) to a sine function suggests that the encounters are nearly uniformly distributed in the solid angle. Hence, the direction of Neptune's spin axis is statistically unimportant.

Then we generate 1000 test moons on prograde circular orbits, all coplanar with respect to the Neptunian equatorial plane (the Neptune-centric frame), with orbits evenly distributed in the range ($10\,R_{\rm Nep}$, $30\,R_{\rm Nep}$). The orbital phase is again randomly drawn. Since the planetary spin axis is essentially unaffected by close encounters (Lee et al. 2007), we assume that Neptune acquires its current obliquity of $\sim$30° before the encounter (by, for example, a giant impact; Morbidelli et al. 2012).

The Sun, IG, Neptune, and 1000 test moons are integrated for 20 yr using MERCURY where the moons are treated as massless particles. During the integration, a moon is removed if it collides with either the IG or Neptune. After the integration, we calculate the orbital elements of the moons in the Neptune-centric frame. A test moon is removed from the simulation if its semimajor axis exceeds half the Neptunian Hill radius (Nesvorný et al. 2003) $R_{\rm Hill} = a_{\rm N}(M_{\rm N}/M_{\rm Sun})^{1/3}$ ($M_{\rm Sun}$ is the solar mass) or if it achieves a hyperbolic orbit. Moons remaining on bound orbits around Neptune are referred to in the following sections as survivors.

2.2. Results

Out of our $500 \times 1000 = 500{,}000$ test moons, 53% survive and their orbital distribution is shown in Figure 4. Not unexpectedly, most have acquired significant eccentricities and inclinations. A small fraction gain orbits with semimajor axes greater than about $100R_{\rm Nep}$, eccentricities up to unity and inclinations up to 180°. Specifically, we observe that the orbits

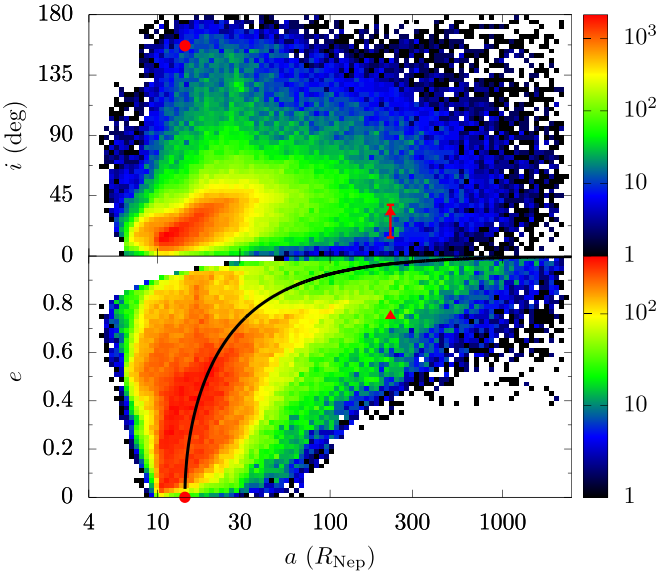

Figure 4. Density histogram of all 2.7×10^5 surviving test particles in Phase 1 that remain bound to Neptune after the IG flyby in the (a, i) and (a, e) planes. Warmer colors represent higher values. The red points and triangles, respectively, mark Triton's and Nereid's present orbit and the error bar shows Nereid's inclination variational range. Note that it is those orbits on the right of Triton's (thus with larger a) that finally evolve toward it later, following equal-angular momentum level curves (black curve in bottom panel).

of both Triton (red circle) and Nereid (red triangle) lie within the distribution of simulated moons.

To determine how well the orbits of the two moons can be reproduced in Phase 1 simulations, we need to quantify how closely a test moon orbit from the simulation should resemble the orbit of the actual satellite. For Nereid ($a = 224R_{\rm Nep}$, $e = 0.75$ and $i = 32°$) we consider those particles injected onto orbits with $a \in (200R_{\rm Nep}, 250R_{\rm Nep})$ as Nereid analogs (NerAs). The time evolution of a typical NerA is shown in column (1) of Figure 5. During the encounter, the NerA is instantly scattered onto a wide, highly eccentric, and inclined orbit, analogous to that of the observed satellite (black triangles on the right).

From the simulations we obtain 1.8×10^3 such NerAs or about $1.8 \times 10^3/5 \times 10^5 \sim 0.4\%$ of the initial prograde satellite population. Because NerAs are defined through a, we show their e and i distribution in the left panel of Figure 6. Here the red region marks the range of eccentricity variation for Nereid and Triton while the vertical and horizontal lines are the median values obtained from NerAs. While the agreement in eccentricity is excellent, the obtained median inclination of the NerAs is somewhat higher but still brackets the observed value to within $1-\sigma_i$ ($\simeq$34°).

Next, we turn our attention to Triton. For reference, Triton has $a = 14.4\,R_{\rm Nep}$, $e \approx 0$, and $i = 157°$. We define test moons on orbits with $i \in (150°, 165°)$ as Triton analogs (TriAs). A typical time evolution of a TriA is presented in column (2) of Figure 5.

We obtain 1.5×10^3 TriAs or about $1.5 \times 10^3/5 \times 10^5 \sim 0.3\%$ of the initial population. Their distribution in a and i is shown in the bottom right panel of Figure 6. Unlike the NerAs matching the observed orbit fairly well, the TriAs immediately after the IG encounter, in general, have wider and more eccentric orbits than the real Triton. Thus, as with Triton's post-capture evolution, additional mechanisms must be invoked to both shrink and circularize the orbit (Goldreich et al. 1989;

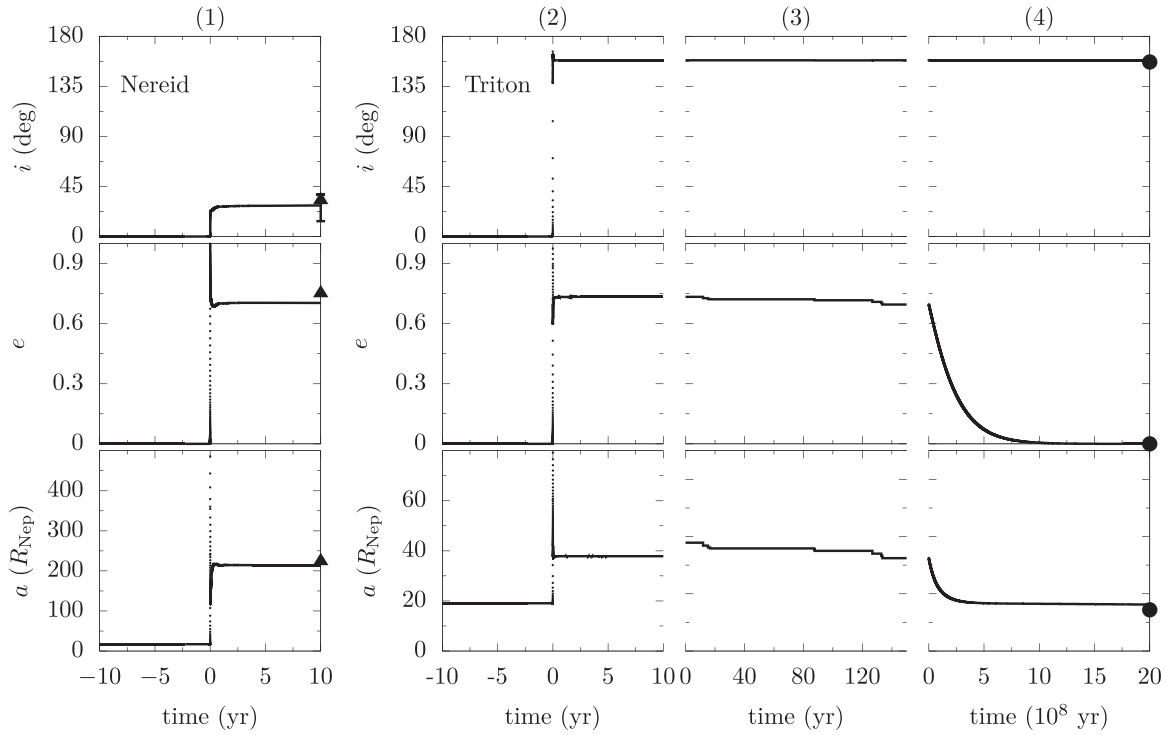

Figure 5. Time evolution of the orbital elements for a Nereid analog (NerA) and a Triton analog (TriA). At time zero (columns 1 and 2) the IG is closest to Neptune. During the encounter, the NerA is directly transferred to a Nereid-like wide and eccentric orbit (1) while, at the same time, the orbit of the TriA is flipped and its eccentricity excited (column 2), causing it to intersect Nereid's. Subsequently, collisions with the other surviving moons rapidly decrease the a and e of the TriA (column 3) while preserving the NerA. Finally, tides circularize the TriA's orbit in ∼Gyr (column 4). Large triangles and circles represent the actual Nereid and Triton.

McKinnon & Leith 1995; Ćuk & Gladman 2005; Correia 2009; Rufu & Canup 2017). We explore these in the next section.

3. Aftermath: Evolution of Circum-Neptunian Material Post-encounter

Following Neptune's encounter with the IG, the surviving satellites will undergo further evolution in the form of mutual gravitational interactions, collisions between each other and with Neptune, and tidal decay of the orbits. The outcome of this phase must satisfy the observational constraints, i.e., the survival of one Triton-sized and one Nereid-sized moon. Gravitational perturbations leading to planetary impact and, to a lesser extent, collisional elimination remove small satellites in Triton-crossing orbits over 10^4–10^5 yr (Ćuk & Gladman 2005; Nogueira et al. 2011), requiring an efficient protection mechanism for Nereid.

We begin to tackle this by considering the "soft" constraint that, for all solar system giant planets, the ratio of the satellites' total mass to that of the host planet, is $\lesssim$0.024% (Canup & Ward 2006; Barr 2017). As Triton itself is already ∼0.02% of the mass of Neptune, it is reasonable to expect exactly one large, Triton-sized moon with the remaining mass of surviving moons (Other Surviving Small Moons or OSSMs) being small enough that Triton survives the ensuing collisional evolution. It has been argued that a head-on impact with an impactor mass of no more than a few percent of Triton's mass would not disrupt Triton (Rufu & Canup 2017). The total mass of OSSMs must satisfy the constraint that $\Sigma m_{\rm OSSM} \lesssim m_{\rm Triton}$, which may be converted into a rough estimate of their number. For instance, if each of the OSSMs is assumed to be of Nereid's mass (∼0.14% of that of Triton; https://ssd.jpl.nasa.gov/?sat_phys_par), there should be no more than several hundred. This is discussed further in Section 4.

We now consider the effect of OSSM–Triton collisions on Triton's orbit. We want to find out how Triton's orbit is altered and at what rate. For this purpose, a system comprised of Neptune, the TriA and a user-defined number of OSSMs is integrated with MERCURY. We run these simulations with 200 OSSMs per TriA, at the high end of the estimated non-Triton mass orbiting Neptune. However, the sole purpose of this exercise is to find out the critical mass—hopefully much lower than the threshold for disruption—of OSSMs needed for orbital decoupling such that the apocenter distance of the TriA becomes smaller than the pericenter distance of the NerA. And, as we will see, the model is not dependent on this particular size frequency distribution (SFD) of the OSSMs so long as their mass is at least a few percent of Triton's.

A TriA is assumed to be of Triton's size and mass (Murray & Dermott 1999) and its starting orbit is taken from the encounter simulations. Each OSSM, assumed to be of Nereid's size and mass, is assigned the median of all prograde orbits from the encounter simulations, a random orbital phase and a random orbit orientation. Mutual gravitational interactions as well as the solar perturbation are omitted (Nogueira et al. 2011), leaving the Neptunian quadrupole term parameterized by the J_2 coefficient (Murray & Dermott 1999). Collisions are treated as perfect mergers with the change in the TriA's orbit calculated via conservation of linear momentum. The integration is terminated as soon as the TriA is decoupled from Nereid's orbit or the simulation reaches 10^4 yr, irrespective of whether decoupling occurs or not.

Not all TriAs need to be examined. As the bottom right panel of Figure 6 shows, only TriAs in the green region can collide with the OSSMs. An orbit outside the green region has a

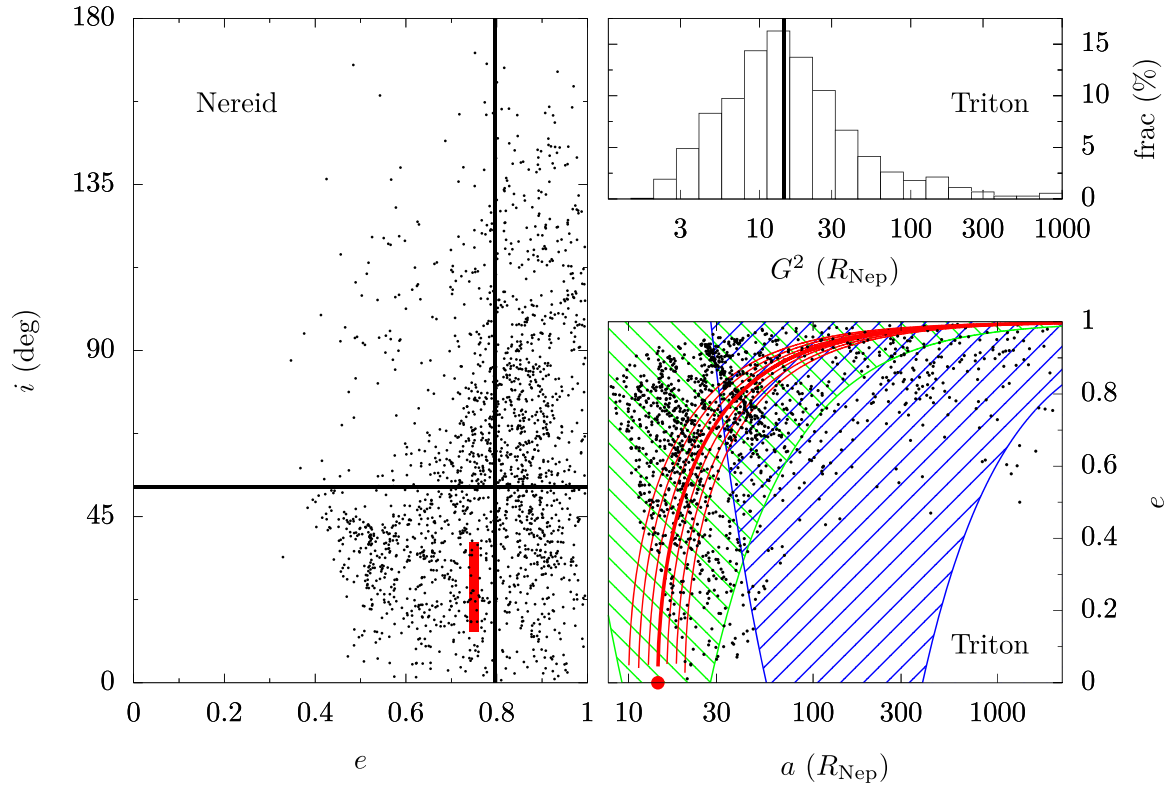

Figure 6. Orbital distribution of the NerAs and TriAs obtained from the encounter simulations. Left: distribution of all the 1.8×10^3 NerAs in the (e, i) plane. The variations of Nereid's actual i and e are shown as the red regions. Black vertical and horizontal lines represent the median e and i of all NerAs. Bottom right: distribution of all the 1.5×10^3 TriAs in the (a, e) plane. Triton is the red circle. A TriA in the blue region may collide with Nereid while one in the green region may collide with the other surviving small moons (see the text). The red curves are level curves of angular momentum, with the thick one corresponding to that of Triton (red point). During collisional and tidal evolution, angular momentum and inclination are quasi-constant and TriAs evolve along the red curves. Top right: histogram of the square of the normalized angular momentum $G^2 = a(1–e^2)$ of all TriAs. The median is 14.1 $R_{\rm Nep}$, ~2% away Triton's value 14.4 $R_{\rm Nep}$ (black vertical line).

pericenter distance larger than the apocenter distance of OSSMs while an orbit outside of the blue region does not pose a risk to the NerA since the orbits do not intersect. Hence, only the 4.9×10^2 TriAs within the intersection of the blue and green regions need to be considered.

An example run is shown in column (3) of Figure 5. In this case, orbit decoupling is achieved over 150 yr after 8 collisions. The timescale is irrelevant; for our purposes, the essential feature of the evolution is that the collisions reduce both a and e and leave i unchanged. From our numerical runs, we find that the TriA's orbit is collisionally decoupled from the NerA's in 96% of cases, typically after colliding with a mass of about 2.7% of Triton's mass (or with about 19 of the OSSMs in the model).

We calculate analytically the collisional timescale $T_{\rm TriA,OSSM}$ between an OSSM and a TriA using the approach of Kessler (1981). We estimate the time to collide with 2.7% of Triton's mass in OSSMs using a truncated harmonic series and find that the time to decouple Triton's orbit is approximately $3.5T_{\rm TriA,OSSM}$ when there are about 20 OSSMs; this is the decoupling timescale. The solid line in Figure 7 shows this timescale as a function of the TriA's semimajor axis. Note that this timescale is weakly dependent on the number of bodies that the mass is divided into (i.e., $\propto \log(N)$) and varies from between $3.5T_{\rm TriA,OSSM} - 8.2T$ and TriA, OSSM when the number of bodies is changed from 20 to 2000 while keeping the total mass constant. Be it $3.5T_{\rm TriA,OSSM}$ or $8.2T_{\rm TriA,OSSM}$, for semimajor axes less than about 100 $R_{\rm Nep}$, it is not more than a few times 10^4 yr (see also Ćuk & Gladman 2005; Rufu & Canup 2017),

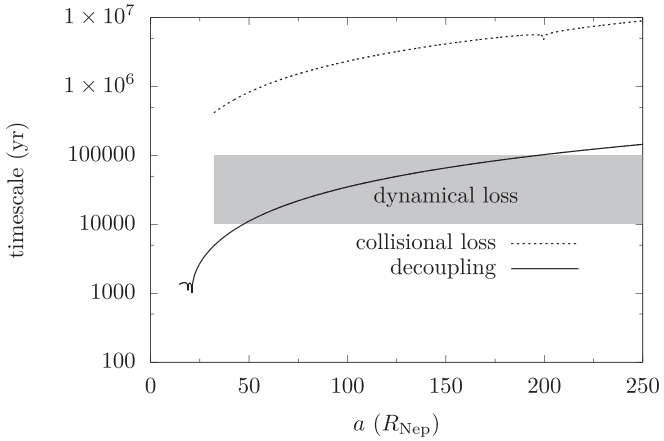

Figure 7. Collisional (dotted line) and dynamical loss (shaded region) timescale for Nereid compared to the decoupling timescale for Triton (solid line). For sufficiently small a, the orbit of the TriA no longer crosses that of the NerA.

comparable to the loss timescale for dynamical interactions by Triton ($\sim 10^4 - 10^5$ yr, shaded region, Ćuk & Gladman 2005; Nogueira et al. 2011). Therefore, the conditions arising after the Neptune-IG encounter favor the survival of Nereid against either dynamical or collisional elimination as long as the TriA acquires an orbit $\lesssim 100\, R_{\rm Nep}$. This is, in fact, true for the vast majority of TriA orbits arising from the encounter phase (Figure 6, bottom right panel).

Therefore, collisions bring down Triton's orbit efficiently enough to preserve Nereid (as well as any other moons on wide orbits; Ćuk & Gladman 2005) and eliminate the OSSMs. As the typical total mass of OSSMs colliding with Triton is only a few percent of Triton's, this moon's angular momentum and inclination remain effectively unchanged.

Our assumption that all OSSMs have the same mass as Nereid is not essential for collisional damping of Triton's orbit. Rather, our model requires that there are some other surviving moons after the IG encounter, and these moons amount to at least a few percent the mass of Triton. Also, the OSSM orbits must be relatively close to Neptune (see Figure 4) such that $T_{\rm TriA,OSSM}$ is smaller than the dynamical lifetime of Nereid.

Following the depletion of the OSSM population, tidal dissipation within the satellites and within the planet further shrinks and circularizes the orbits (panels 3 and 4 of Figure 2).

Nereid's orbit is too far from Neptune to be significantly affected by tides and is not considered further in the following. Triton's tidal evolution has been discussed extensively in the literature (McKinnon 1984; Chyba et al. 1989; Goldreich et al. 1989; McKinnon et al. 1995; Ćuk & Gladman 2005; Correia 2009; Nogueira et al. 2011). Here we want to know specifically the effect of tides on the orbit of the TriA following collisional evolution. For this purpose, we follow a recent implementation (Correia 2009) of the equilibrium tidal model (Hut 1981). Since the orbit of a TriA is now entirely inside that of Nereid, orbital precession is controlled by Neptune's oblateness (Goldreich et al. 1989; Nogueira et al. 2011; Li & Christou 2016) and the solar perturbation may be omitted. Actually, we can also disregard the planetary oblateness, as it causes orbital precession but not secular variations in a, e, or i (Nogueira et al. 2011). We consider the TriA as a rocky body with Love number $k_{\rm Tri} = 0.1$ and tidal $Q_{\rm Tri} = 100$ (Goldreich et al. 1989; Correia 2009; Nogueira et al. 2011); the solid body parameters for Neptune are taken from Correia (2009) and Hubbard et al. (1991).

A typical TriA evolution is shown in column (4) of Figure 5. As with collisions, i is unaffected while both a and e decrease and the orbital angular momentum is quasi-conserved. Here the orbit of the TriA is circularized within a gigayear, consistent with other studies (Goldreich et al. 1989; Correia 2009; Nogueira et al. 2011). This timescale is shorter if the TriA is molten or semimolten (McKinnon 1984; Goldreich et al. 1989; Nogueira et al. 2011). In fact, for any TriA with pericenter distance $q < 20R_{\rm Nep}$, tides circularize the orbit within the age of the solar system (Nogueira et al. 2011).

4. Discussion

4.1. Comparison with Observations and Model Efficiency

We first examine how well our model matches the observed orbits of Triton and Nereid.

Since its orbit is circular, Triton is defined by its orbital i and a. In our model, both i and the normalized angular momentum G are quasi-conserved during collisional as well as tidal evolution and are thus determined solely from the IG-encounter phase. By definition, all TriAs have inclinations close to Triton's; therefore, we only need to consider G. In the top right panel of Figure 6, we show that the median of G^2 of our TriAs is within 2% of the observed value, suggesting that our model reproduces the correct final orbit for Triton.

On the other hand, a NerA is directly placed onto a wide, highly eccentric orbit during the encounter phase and experiences no further evolution. By definition, NerAs all have a similar to Nereid's. As shown in the left panel of Figure 6, the median e of the NerAs is 0.80, ∼6% from that observed. The dispersion in i of the NerAs is large and Nereid is within $1\text{–}\sigma_i$.

The efficiency of our model is determined mainly by the Neptune-IG encounter phase because the outcome of subsequent evolution—producing a Triton-like object with orbit circularized within the age of the solar system—is fairly deterministic and the NerA does not participate in the latter phase.

The simulation results indicate that about 1.8×10^3 of the initial 5×10^5 prograde satellite particles ended up on Nereid-like orbits after the encounter with the ice giant and are labeled as NerAs. This suggests that the probability of an object with Nereid's orbit and size resulting from a similarly deep encounter is $P_{\rm NerA} \sim 4 \times 10^{-3} N_{R>R_{\rm Nereid}}$, where $N_{R>R_{\rm Nereid}}$ is the number of Nereid-sized moons ($R_{\rm Nereid} \simeq 170$-km) in the initial satellite system. If there were a few tens of these moons $N_{R>R_{\rm Nereid}} \sim 20$ in the primordial system, the probability of an encounter producing a NerA is about $P_{\rm NerA} \sim 0.1$. Similarly, when examining the encounter results we find that 1.5×10^3 of the 5×10^5 initial prograde satellite particles are transferred to orbits with Triton-like retrograde orbits and are labeled as TriAs. This suggests that the probability of an object with Triton's inclination and size resulting from a deep encounter is about $P_{\rm TriA} \sim 3 \times 10^{-3} N_{R>1000\,{\rm km}}$, where $N_{R>1000\,{\rm km}}$ is the number of large ($R > 1000$ km) satellites in the initial prograde satellite population. Another factor is that the chance of a 0.003 au encounter happening is ∼0.1 (Deienno et al. 2014; Nesvorný et al. 2014b). Hence, the overall success rate of our model to account for both Triton and Nereid in this way is about 3×10^{-5}.

Clearly, how stringently we define TriAs and NerAs has a great impact on the model efficiency. If we only ask the TriAs to have an inclination $i > 90°$ instead of $i \in (150°, 165°)$, the chance for creating one such object increases by a factor of 10 to 3%. Similarly, if all orbits with $a > 100\,R_{\rm Nep}$ are recognized as NerAs rather than requiring $a \in (200R_{\rm Nep}, 250R_{\rm Nep})$, the corresponding rates also rise by an order of magnitude, also reaching 3%. Combined, this suggests that if the analogs are loosely defined, the overall efficiency reaches a few times 10^{-3}.

4.2. Comparison with Capture Models

In situ formation models for the two moons have been discussed in Section 1, so here we focus on capture models. A leading mechanism for Triton's capture is via a three-body encounter (Agnor & Hamilton 2006). In this model, Triton and a bound massive binary companion encounter Neptune. During this encounter the orbit of the binary is tidally disrupted and leaves the Triton-mass object on a bound orbit around Neptune, while its companion escapes on a hyperbolic trajectory. The capture efficiency, examined in the context of the Nice scenario, has been estimated to be between 2% (Vokrouhlický et al. 2008) and 50% (Nogueira et al. 2011); though, this exchange capture may have occurred before the Nice scenario with a higher efficiency (Vokrouhlický et al. 2008). Hence, in terms of Triton's procurement alone, our model is less likely than capture via three-body gravitational encounters

(Agnor & Hamilton 2006; Vokrouhlický et al. 2008; Nogueira et al. 2011).

However, Nereid's acquisition is also nontrivial. Nereid is the largest among the so-called irregular satellites (Figure 1) and larger than Trojan asteroids, populations genetically linked in that they were both captured by the giant planets during the instability period from the PPD (Nesvorný et al. 2013, 2007, 2014a). The largest Jovian Trojan (624) Hektor and irregular moon (J VI) Himalia have been used to show the consistency between capture efficiencies and the SFD and the total mass of the PPD (Nesvorný & Vokrouhlický 2016). However, Nereid does not readily fit into this picture. For example, Hektor, the second largest object within the two populations, is 230 km in diameter (Nesvorný & Vokrouhlický 2016) and its capture efficiency, as a Trojan at Jupiter, is (6–8) $\times$ 10^{-7} (Nesvorný et al. 2013), $\sim$20 times higher than the capture of irregular satellites at Neptune (Nesvorný et al. 2014a). Furthermore, the steep SFD (Nesvorný & Vokrouhlický 2016) implies Nereid-sized (or larger) objects are rarer than Hektor by almost an order of magnitude. These facts combined suggest that the capture of Nereid is $\sim$100 times as infrequent as that of Hektor: should capturing one Hektor-sized object on Jovian Trojan orbits be expected (Nesvorný & Vokrouhlický 2016), acquiring one Nereid-sized body at Neptune must be unlikely. Indeed, following these works, the expected number of such large objects captured at Neptune is $<$0.006.

In summary, the chance of capturing both Triton (Agnor & Hamilton 2006) and Nereid (Nesvorný et al. 2007) is thus 10% $\times$ 0.6% $\sim$ 6 $\times$ 10^{-4}, higher than the average efficiency of our model by a factor of 10. We note that capture models do not strongly constrain the characteristics of the capture orbit. Leaving Triton aside, Nereid has the largest orbital eccentricity and the smallest semimajor axis (in units of the host planet's Hill radius) among all irregular moons (Figure 1). Indeed, Nereid is located at the inner edge of the region where the capture mechanism operates (Nesvorný et al. 2007, 2014a). As discussed before, our efficiency reaches a few times 10^{-3} if we loosen the requirement on the orbital similarity between the observation and the analogs and this is higher than that of the capture models by a factor of a few.

However, the origin of the two moons may not be related at all. For example, Triton may be captured long before Nereid is captured and when the latter arrives, the orbit of the former has already been small enough—no issue for the stability of Nereid. Then it is perhaps unfair to compare the overall efficiency between the in situ and the capture models and only the success rate for the individual satellites should be compared. As discussed before, the exchange capture model for Triton is probably better while our model seems to work particularly well for Nereid. So can the two work together? Timing is important. If Triton predates Nereid, upon capture Triton gains a highly eccentric orbit of which the circularization would probably have cleared any small moons, leaving no seeds for Nereid anymore. Also, Triton itself may be excited or even ejected by the encounter. Alternatively, if Nereid precedes Triton, during the encounter Nereid was placed onto its current orbit with some other small moons surviving. Then when Triton is captured, it collides with these other moons and Nereid is protected. So it seems that (2) may be viable but detailed modeling is needed to confirm this.

4.3. The Primordial Satellite Population

The scenario advocated here operates with an efficiency of $\sim$$10^{-5}$ in a self-contained and self-consistent way, reproducing the main orbital features of both Triton and Nereid. Here we discuss its principal weaknesses.

Firstly, how realistic is the assumed size distribution of the initial satellite population? This has been constructed based on the known inventory of solar system moons and our model efficiency (Section 2).

Currently, Jupiter and Uranus each has four large, similar-sized moons plus smaller ones.[3] Perhaps the system most closely resembling our assumed configuration is that of Saturn where the mass budget is dominated by Titan together with several intermediate-sized moons (each of 0.5%–1.7% of Titan's mass; https://sites.google.com/carnegiescience.edu/sheppard/moons/saturnmoons) but only a few, hundred-kilometer-sized moons. So, small number statistics aside, it seems that our assumption on the initial size distribution of Neptune moons does not have concrete observational support. However, available to us are only the satellites' current configurations: e.g., moons exterior to Uranus' outermost moon Oberon could have been lost (Deienno et al. 2011) and may not necessarily be primordial.

While the assumption that one Triton-sized moon exists seems sensible at least mass-wise (Barr 2017; Szulágyi et al. 2018), the number of smaller moons, a few tens, is estimated from the expectation that one Nereid should be created during the best encounters (those featuring the highest occurrence rates of TriAs and NerAs). A few tens of such moons, under these encounters, give rise to a NerA at an efficiency close to unity and, fortuitously, provide just the right amount of impacting mass to shrink the orbit of the TriA (its creation still a small-likelihood event) quickly enough to protect the NerA without disrupting the TriA. Nonetheless, when estimating the number of small moons using the overall creation efficiency for the NerA ($\sim$0.1%), an initial population of a few hundred results. These moons, if each of Nereid's mass, total $\sim$10% of that of Triton. While more efficiently decoupling Triton from Nereid, this population's large total mass implies a considerable decrease in the normalized angular momentum G of Triton. Thus, our argument about the agreement between the observed value and simulations fails (top right panel of Figure 6). On the other hand, if only a few moons exist before the encounter it would be difficult to create a NerA and its survival becomes problematic.

Finally, we comment on the implications for Neptune's remaining moons. The irregular satellites are omitted from our discussion as these moons may have been acquired by Neptune later on (Nesvorný et al. 2007). The inner regular moons, however, will be perturbed by the IG. To quantify the maximum possible extent of the perturbation, we consider Proteus, the inner neighbor of Triton at 4.7 $R_{\rm Nep}$. For each of our 500 encounters, we place 10 test moons at 5 $R_{\rm Nep}$ around Neptune and follow them through the encounter. We observe that all these 500 $\times$ 10 = 5000 moons are stable and their orbital excitation is small, with a median eccentricity $\lesssim$0.04. Moreover, because this moon is prograde and outside the synchronous orbit, it must have migrated outwards in the past. Therefore, Proteus has been closer to Neptune during our encounter and should have been disturbed to an even smaller

[3] But we do note that such four-moon systems may turn into ones containing a single large moon plus others (Asphaug & Reufer 2013).

degree. This experiment represents a worst-case-scenario for the disturbance to the inner regular satellites. Yet, these moons may also be perturbed by Triton, gaining moderate eccentricities which accelerates the rate of internal tidal dissipation (Rodríguez et al. 2011) or leads to disruptive collisions between Proteus and others (Banfield & Murray 1992).

5. Conclusions and Implications

We have explored an in situ combined formation scenario for two peculiar moons in the Neptunian system: Triton and Nereid. In our model, both moons formed in a circum-Neptunian disk, together with another set of tens of small moons. A close encounter between Neptune and an ice giant, penetrating down to the satellite system, flips the orbit of Triton and places Nereid onto a wide and eccentric orbit. Nereid's orbit immediately following this event matches observations well, but Triton's is too large and eccentric. Then, collisions between Triton and the other small moons shrink Triton's orbit on 10^4 yr timescales. This removes the small moons and protects Nereid from elimination by Triton. Finally, tides circularize Triton's orbit over gigayears. Our self-contained model explains the major orbital features of both Triton and Nereid.

We note that the only exomoon candidate known so far resides on an orbit tilted by $\sim(42 \pm 18)^\circ$ with respect to that of its host planet (Teachey & Kipping 2018). While further observations are needed to confirm its orbital parameters, the mechanism we propose here for solar system moons suggests an evolutionary pathway for such high-inclination satellites. Given the ubiquity of dynamical instability among exoplanets (Rasio & Ford 1996; Gong et al. 2013), we predict a plethora of exomoons on highly excited orbits produced during planetary encounters. Similarly, planets are themselves subject to the disturbance of stellar encounters so, as shown here for Triton and Nereid, a planet can be injected on a highly eccentric, inclined and/or distant orbit by such events (Malmberg et al. 2011; Li et al. 2019).

The authors are grateful to the anonymous referee for useful comments. The authors thank Dr. Craig B. Agnor for discussions and comments as well as direct text editing of the manuscript; his remarks have led to changes to the paper structure and content, including a more comprehensive discussion on collisional evolution.

D.L. thanks Anders Johansen, Douglas Hamilton, David Nesvorný, and Matija Ćuk for useful discussions. D.L. acknowledges the Knut and Alice Wallenberg Foundation through two grants (2014.0017, PI: Melvyn B. Davies and 2012.0150, PI: Anders Johansen). Computations were carried out at the center for scientific and technical computing at Lund University (LUNARC) through the Swedish National Infrastructure for Computing (SNIC) via project 2018/3-314. Astronomical research at the Armagh Observatory and Planetarium is funded by the Northern Ireland Department for Communities (DfC).

ORCID iDs

Daohai Li https://orcid.org/0000-0002-8683-1758

References

Agnor, C. B., & Hamilton, D. P. 2006, Natur, 441, 192
Agnor, C. B., & Lin, D. N. C. 2012, ApJ, 745, 143
Asphaug, E., & Reufer, A. 2013, Icar, 223, 544
Banfield, D., & Murray, N. 1992, Icar, 99, 390
Barr, A. C. 2017, AstRv, 12, 24
Batygin, K., Brown, M. E., & Betts, H. 2012, ApJL, 744, L3
Brasser, R., Morbidelli, A., Gomes, R., Tsiganis, K., & Levison, H. F. 2009, A&A, 507, 1053
Canup, R. M., & Ward, W. R. 2006, Natur, 441, 834
Chambers, J. E. 1999, MNRAS, 304, 793
Chyba, C. F., Jankowski, D. G., & Nicholson, P. D. 1989, A&A, 219, L23
Cloutier, R., Tamayo, D., & Valencia, D. 2015, ApJ, 813, 8
Colombo, G., & Franklin, F. 1971, Icar, 15, 186
Correia, A. C. M. 2009, ApJ, 704, L1
Ćuk, M., & Burns, J. A. 2004, Icar, 167, 369
Ćuk, M., & Gladman, B. J. 2005, ApJ, 626, L113
Dawson, R. I., & Murray-Clay, R. 2012, ApJ, 750, 43
Deienno, R., Nesvorný, D., Vokrouhlický, D., & Yokoyama, T. 2014, AJ, 148, 25
Deienno, R., Yokoyama, T., Nogueira, E. C., Callegari, N., & Santos, M. T. 2011, A&A, 536, A57
Farinella, P., Milani, A., Nobili, A. M., & Valsecchi, G. B. 1980, Icar, 44, 810
Fernández, J. A., & Ip, W. H. 1984, Icar, 58, 109
Goldreich, P., Murray, N., Longaretti, P. Y., & Banfield, D. 1989, Sci, 245, 500
Gomes, R., Nesvorný, D., Morbidelli, A., Deienno, R., & Nogueira, E. 2018, Icar, 306, 319
Gong, Y.-X., Zhou, J.-L., Xie, J.-W., & Wu, X.-M. 2013, ApJ, 769, L14
Harrington, R. S., & Van Flandern, T. C. 1979, Icar, 39, 131
Heppenheimer, T. a., & Porco, C. 1977, Icar, 30, 385
Hubbard, W. B., Nellis, W. J., Mitchell, A. C., et al. 1991, Sci, 253, 648
Hut, P. 1981, A&A, 99, 126
Kessler, D. J. 1981, Icar, 48, 39
Lee, M. H., Peale, S. J., Pfahl, E., & Ward, W. R. 2007, Icar, 190, 103
Li, D., & Christou, A. A. 2016, CeMDA, 125, 133
Li, D., Mustill, A. J., & Davies, M. B. 2019, MNRAS, 488, 1366
Malhotra, R. 1993, Natur, 365, 819
Malmberg, D., Davies, M. B., & Heggie, D. C. 2011, MNRAS, 411, 859
McKinnon, W. B. 1984, Natur, 311, 355
McKinnon, W. B., & Leith, A. C. 1995, Icar, 118, 392
McKinnon, W. B., Lunine, J. I., & Banfield, D. 1995, in Neptune and Triton, ed. D. Cruikshank (Tucson, AZ: Univ. Arizona Press), 807
Minton, D. a., & Malhotra, R. 2011, ApJ, 732, 53
Morbidelli, A., Brasser, R., Gomes, R., Levison, H. F., & Tsiganis, K. 2010, AJ, 140, 1391
Morbidelli, A., Brasser, R., Tsiganis, K., Gomes, R., & Levison, H. F. 2009, A&A, 507, 1041
Morbidelli, A., Gaspar, H. S., & Nesvorny, D. 2014, Icar, 232, 81
Morbidelli, A., Tsiganis, K., Batygin, K., Crida, A., & Gomes, R. 2012, Icar, 219, 737
Murray, C. D., & Dermott, S. F. 1999, Solar System Dynamics (Cambridge: Cambridge Univ. Press)
Nesvorný, D. 2015, AJ, 150, 68
Nesvorný, D., Alvarellos, J. L. A., Dones, L., & Levison, H. F. 2003, AJ, 126, 398
Nesvorný, D., & Morbidelli, A. 2012, AJ, 144, 117
Nesvorný, D., & Vokrouhlický, D. 2016, ApJ, 825, 94
Nesvorný, D., Vokrouhlický, D., & Deienno, R. 2014a, ApJ, 784, 22
Nesvorný, D., Vokrouhlický, D., Deienno, R., & Walsh, K. J. 2014b, AJ, 148, 52
Nesvorný, D., Vokrouhlický, D., & Morbidelli, A. 2007, AJ, 133, 1962
Nesvorný, D., Vokrouhlický, D., & Morbidelli, A. 2013, ApJ, 768, 45
Nicholson, P. D., Ćuk, M., Sheppard, S. S., Nesvorný, D., & Johnson, T. V. 2008, in The Solar System Beyond Neptune, ed. M. A. Barucci et al. (Tucson, AZ: Univ. Arizona Press), 411
Nogueira, E., Brasser, R., & Gomes, R. 2011, Icar, 214, 113
Pollack, J. B., Tauber, M. E., & Burns, J. A. 1979, Icar, 37, 587
Rasio, F. A., & Ford, E. B. 1996, Sci, 274, 954
Rodríguez, A., Ferraz-Mello, S., Michtchenko, T. A., Beaugé, C., & Miloni, O. 2011, MNRAS, 415, 2349
Rufu, R., & Canup, R. M. 2017, AJ, 154, 208
Szulágyi, J., Cilibrasi, M., & Mayer, L. 2018, ApJ, 868, L13
Teachey, A., & Kipping, D. M. 2018, SciA, 4, eaav1784
Tsiganis, K., Gomes, R., Morbidelli, A., & Levison, H. F. 2005, Natur, 435, 459
Vokrouhlický, D., Nesvorný, D., & Levison, H. F. 2008, AJ, 136, 1463
Wolff, S., Dawson, R. I., & Murray-Clay, R. A. 2012, ApJ, 746, 171